Partial Mural Cell Ablation Disrupts Coronary Vasculature Integrity and Induces Systolic Dysfunction

Lauriane Cornuault, François-xavier Hérion, Célia Bourguignon, Paul Rouault, Ninon Foussard, Philippe Alzieu, Candice Chapouly, Alain-pierre Gadeau, Thierry Couffinhal, Marie-ange Renault

Title

Partial mural cell ablation disrupts coronary vasculature integrity and induces systolic dysfunction.

Authors and affiliations

Lauriane Cornuault, PhD[1], François-Xavier Hérion, MD[1], Célia Bourguignon, MS[1], Paul Rouault, MS[1], Ninon Foussard, MD[1], Philippe Alzieu, BS[1], Candice Chapouly, PharmD, PhD[1], Alain-Pierre Gadeau, PhD[1], Thierry Couffinhal , MD, PhD[1] and Marie-Ange Renault, PhD[1]

[1] Univ. Bordeaux, Inserm, Biology of Cardiovascular Diseases, U1034, CHU de Bordeaux, F-33604 Pessac, France

Running title

Pericytes preserve cardiac function

Corresponding author

Marie-Ange Renault

Inserm U1034

1, avenue de Magellan

33604 Pessac

France

e-mail : marie-ange.renault@inserm.fr

Tel : (33) 5 57 89 19 79

Abstract

Background: While the critical role of pericytes in maintaining vascular integrity has been extensively demonstrated in the brain and the retina, little is known about their role in the heart. We aim to investigate structural and functional consequences of partial pericyte depletion (about 60%) in the heart of adult mice. **Methods and Results**: To deplete pericyte in adult mice, we used Pdgfrb-Cre/ERT2; $Rosa^{DTA}$ mice and compared their phenotype to the one of control mice ($Rosa^{DTA}$) chosen among their littermates. Cardiac function was assessed via echocardiography and left ventricle (LV) catheterization one month after the first tamoxifen injection. Mice depleted with pericytes displayed increased coronary endothelium leakage and activation, which was associated with increased CD45 + cell infiltration in the heart. Pericyte depletion also modified the phenotype of cardiomyocytes with an increased expression of Myosin Heavy Chain 7 and decreased expression of ATPase Sarcoplasmic/Endoplasmic Reticulum Ca2+ Transporting 2 and Connexin-43. As a consequence, mice depleted with pericytes had a reduced LVEF and an increased end-diastolic pressure, demonstrating both systolic and diastolic dysfunction. Consistently, mice depleted with pericytes presented a decreased LV contractility and an increased LV relaxation time (dP/dt_{min}). Besides, this study reveals that cardiac pericytes may undergo strong remodeling upon injury. **Conclusions**: Cardiac pericyte depletion induces both systolic and diastolic dysfunction, suggesting that pericyte dysfunction may contribute to the occurrence of cardiac diseases.

Keywords

Pericytes, heart, coronary micro-vasculature, cardiac function

Clinical Perspective

What Is New?

- The present study demonstrates cardiac pericytes are critical to maintain proper cardiac function.
- Cardiac pericytes modulate the properties of cardiomyocytes directly, notably CX43 expression level.
- Cardiac pericytes prevent cardiac inflammation by downregulating Il-6 in both ECs and cardiomyocytes.

What Are the Clinical Implications?

- Cardiac pericytes should be taken into account when investigating the pathophysiology of cardiac disease.

Research Perspective

What New Question Does This Study Raise?

- Do cardiac pericyte participate in the pathophysiology of cardiac diseases notably heart failure

What Question Should be Addressed Next?

- How is the phenotype of cardiac pericyte modified by cardiovascular risk factor?

Non-standard Abbreviations and Acronyms

PDGFRB: Platelet Derived Growth Factor Receptor Beta

DTA: diphtheria toxin A

PDGFB: Platelet-derived growth factor submit B

LVEF: left ventricular ejection fraction

ProNGF: pro-Nerve growth factor

Notch3: Notch Receptor 3

ZSF1: Zucker fatty/spontaneously hypertensive heart failure F1 hybrid

SARS-CoV-2: Severe acute respiratory syndrome coronavirus 2

lncRNA: Long Non-coding

LV: Left-ventricular

ESV: end-systolic volume

EDV: end-diastolic volume

LVPW: left ventricular posterior wall

IVS: inter-ventricular septum

LVID: Left ventricular internal diameter

HDL: high density lipoproteins

LDL: Low density lipoproteins

PODXL: Podocalyxin

SMA: anti–alpha-smooth muscle actin (also known as ACTA2)

NG2: Chondroitin Sulfate Proteoglycan 4 (also known as CSPG4)

CDH5: Cadherin-5

FGB: Fibrinogen B chain

WGA: Wheat Germ Agglutinin

HRP: Horseradish peroxidase

DAB: diaminobenzidine

DAPI: (4’,6-diamidino-2-phenylindole)

EBM-2: Endothelial basal medium-2

HMVEC-C: Human cardiac microvascular endothelial cells

EGM: Endothelial growth medium

MEM: Minimum Essential Medium

ATP: Adenosine Triphosphate

RT-qPCR: Real-time quantitative polymerase chain reaction

ICAM1: Intercellular Adhesion Molecule 1

VCAM1: Vascular Cell Adhesion Molecule 1

ATP2A2: ATPase sarcoplasmic/endoplasmic reticulum Ca2+ transporting 2

PAGE: Polyacrylamide gel electrophoresis

PLN: Phospholamban

Ser: Serine

Thr: Threonin

TUBA1A: Tubulin Alpha 1a

smMHC: Smooth muscle myosin heavy chain (aslo known as MYH11)

SMC: Smooth muscle cell

EC: endothelial cell

VIM: Vimentin

Col1a1: Collagen Type I Alpha 1 Chain

Col3a1: Collagen Type III Alpha 1 Chain

Tgfb1: Transforming Growth Factor Beta 1

Ctgf: Connective Tissue Growth Factor (also known as CCN2)

CDH2: Cadherin-2

CX43: Connexin 43 (also known as GJA1)

Ttn: Titin

Myh7: Myosin Heavy Chain 7

DTR: diphtheria toxin receptor

HIF1A: Hypoxia Inducible Factor 1 Subunit Alpha

Introduction

Pericytes are cells that reside in the microvasculature and share a basement membrane with the underlying endothelial cells (ECs). Pericyte density varies between different organs. In the brain, the organ with the highest density of pericytes; the EC–pericyte ratio varies between 1:1 and 3:1 [1]. Accordingly, the brain is also the organ in which the role of pericyte has been the most investigated. Notably, in this organ, pericytes are thought to play a role in regulating permeability across the blood–brain barrier [2,3] since mice deficient in pericytes or exhibiting decreased pericyte function have increased vascular permeability [2,3]. Notably, pericyte function and maintenance depends on Platelet-derived growth factor submit B (PDGFB) expression by quiescent adult microvascular brain endothelium [4].

The pericyte content of the cardiac micro-vasculature is thought to be closer to the one of the cerebral vasculature, with an endothelial–pericyte ratio of 2:1–3:1 [5]. It is also likely that pericytes contribute to the maintenance of microvascular function in the heart given that the loss of pericytes has been associated with increased vascular permeability [6 7], endothelial activation [7] and altered vasomotricity [6]. Notably, in mice treated with PDGF receptor inhibitors (sunitinib and CP-673451), decreased pericyte coverage of cardiac capillaries was associated with increased permeability, impaired endothelium-dependent vasodilation and decreased coronary flow reserve [6]. Besides, the expression of a mutant form of pro-Nerve growth factor (ProNGF), unable to be matured and which may target pericytes, was shown to induce endothelial activation and vascular leakage [7]. Finally, pericyte loss observed in both Sirtuin 3 [8] and Notch Receptor 3 (*Notch3*) [9] deficient mice was associated with decreased coronary flow reserve. Importantly, in each of these studies, impaired microvascular integrity and function has been also associated with cardiac dysfunction. Notably, administration of the PDGF receptor-specific inhibitor CP-673451 was shown to decrease left ventricular ejection fraction (LVEF) [6], expression of the mutant form of ProNGF induced dilated cardiomyopathy, cardiac fibrosis, and contractile dysfunction [7], Sirtuin 3 deficient mice showed decreased EF and fractional shortening after myocardial infarction [8] while *Notch3* deficient mice were shown to exhibit cardiac hypertrophy [9]. Altogether these studies suggest that pericytes may be beneficial to the coronary vasculature which may have a direct or indirect impact on cardiac function. However, in the heart, pericytes were also proposed to have deleterious effects. Notably, pericytes may become myofibroblasts and contribute to fibrosis. [10]. Also, capillary pericytes are suggested to be responsible for coronary no-reflow after myocardial ischemia by inducing capillary constriction [11] via a mechanism involving G Protein-Coupled Receptor 39 [12].

In pathophysiological conditions, cardiac pericytes have been shown to either decrease or increase in number. Loss of pericytes has been shown to constitute a remarkable feature of aging in several organs including the heart in both mice and humans [13]. Also, high-fat diet was shown to induce pericyte loss in the heart of mice [14]. On the contrary, cardiac pericytes were shown to be disorganized and more numerous in Zucker fatty/spontaneously hypertensive heart failure F1 hybrid (ZSF1) rats [15]. In other conditions, such as Severe acute respiratory syndrome coronavirus 2 (SARS-CoV-2) infection, the phenotype of pericytes is proposed to be modified by the acquisition of a more contractile phenotype [16]. Finally, pericyte dedifferentiation leading to increased endothelial

permeability is proposed to be induced by the downregulation of Hypoxia-Induced Endoplasmic Reticulum Stress Regulating lncRNA in human heart failure [17].

In conclusion, cardiac pericytes may participate in the pathophysiology of cardiac diseases through a wide range of mechanisms. However, studies performed so far are mainly descriptive and their conclusions are based on associations. The purpose of the present study is to investigate the specific consequences of pericyte depletion on cardiac structure and function.

Methods

The authors declare that all supporting data are available within the article and its online supplementary files. Also, we used the ARRIVE reporting guidelines [18].

Mice

B6.Cg-Tg(Pdgfrb-cre/ERT2)6096Rha/J (strain# 029684), Gt(ROSA)26Sortm4(ACTB-tdTomato,-EGFP)Luo/J (Strain # 007576) (named $Rosa^{mTmG}$ in the manuscript) and B6.129P2-Gt(ROSA)26Sortm1(DTA)Lky/J (Strain#009669) (naimed $Rosa^{DTA}$ in the manuscript) were obtained from the Jackson laboratory.

Pdgfrb-cre/ERT2 mice were crossed with $Rosa^{DTA/DTA}$ mice to obtain Pdgfrb-CreERT2; $Rosa^{DTA}$/+ (Pdgfrb-DTA) mice and control $Rosa^{DTA}$/+ mice.

Pdgfrb-cre/ERT2 mice were crossed with $Rosa^{mTmG/mTmG}$ mice to obtain Pdgfrb-CreERT2; $Rosa^{mTmG}$/+ mice.

The Cre recombinase in Pdgfrb-Cre/ERT2 mice was activated by intraperitoneal injection of 50 mg/kg/day tamoxifen (Sigma-Aldrich) for 5 consecutive days at 8 weeks of age and eventually repeated 2 weeks later at 10 weeks of age.

Animal were house in a conventional animal facility. Animal experiments were performed in accordance with the guidelines from Directive 2010/63/EU of the European Parliament on the protection of animals used for scientific purposes and approved by the local Animal Care and Use Committee of Bordeaux University. The appearance, weight, clinical signs and the behavior of the mice were monitored every day in order to prevent animal pain and distress. Both males and females were used. The number of animals per group necessary to have a 90% chance to find a significant difference between 2 groups was calculated using G power 3.1 software. The calculation was made for the measurement of cardiac function (notably LVEF). Mice were either sacrificed by cervical dislocation or exsanguination under deep anesthesia (ketamine 100 mg/kg and xylazine 20 mg/kg, IP). A total of 60 mice were used in the study. No animal were excluded from the study.

Echocardiography

Left-ventricular (LV) EF and LV dimension were measured on a high-resolution echocardiographic system equipped with a 30-MHz mechanical transducer (VEVO 2100, VisualSonics Inc.) as previously described [19,20]. Mice were anchored to a warming platform in a supine position, limbs were taped to the echocardiograph electrodes, and chests were shaved and cleaned with a chemical hair remover to minimize ultrasound attenuation. UNI'GEL ECG (Asept Inmed), from which all air bubbles had been expelled, was applied to the thorax to optimize the visibility of the cardiac chambers. LVEF were evaluated by planimetry as recommended [21]. Two-dimensional, parasternal long-axis and short-axis views were acquired, and the endocardial area of each frame was calculated by tracing the endocardial limits in the long-axis view, then the minimal and maximal areas were used to determine the left-ventricular end-systolic (ESV) and end-diastolic (EDV) volumes, respectively. The system software uses a formula based on a cylindrical-hemiellipsoid model (volume=8.area²/3π/ length) [22]. The LVEF was derived from the following formula: (EDV- ESV)/EDV*100. The cardiac wall thickness, left ventricular posterior wall (LVPW), inter-ventricular septum (IVS) and left ventricular internal diameter (LVID) were calculated by tracing wall limits in both the long and short axis views.

LV pressure /systolic blood pressure measurement

LV diastolic pressure measurement was assessed via an invasive catheterization technique. Mice were anesthetized with Isoflurane. A Scisense pressure catheter (Transonic) was inserted into the LV through the common carotid artery. Pressure was recorded using LabChart software. End diastolic pressure, dP/dt minimum and maximum, Tau and heart rate were automatically calculated by a curve fit through end-systolic and end-diastolic points on the pressure plot.

Blood sampling for biochemical marker analysis/NFS

Blood samples were collected by the heparin retroorbital bleeding method at sacrifice. Blood cell counts were determined using an automated counter (scil Vet abc Plus+). Plasma was separated by a 10-min centrifugation at 2500 g and then stored at -80°C. Concentrations of the following biomarkers were measured using an Architect CI8200 analyzer (Abbott Diagnostics, North Chicago, Illinois, USA): triglycerides, using the lipoprotein-lipase/glycerol kinase/oxidase/peroxidase method; total cholesterol, using the esterase/oxidase/peroxidase method; and high density lipoproteins (HDL) cholesterol, using the accelerator/selective detergent/esterase/oxidase/peroxidase method. Low density lipoproteins (LDL) cholesterol was then estimated using the Friedewald formula (LDL cholesterol [mmol/L] = total cholesterol – HDL cholesterol – [triglycerides/2,2], or LDL cholesterol [mg/dL] = total cholesterol – HDL cholesterol – [triglycerides/5]).

Tissue staining/Immunostaining

ECs were identified using anti-CD31 or anti-Podocalyxin (PODXL) antibodies or Biotin-conjugated Isolectin B4 (Vector). Muscularized vessels were identified using anti–alpha-smooth muscle actin (SMA) antibodies. Pericyte were identified using anti-Chondroitin Sulfate Proteoglycan 4 (CSPG4 also known as NG2) or anti- Platelet Derived Growth Factor Receptor Beta (PDGFRB) antibodies.

Leucocyte, macrophage, T-cell and B-cell infiltrations were quantified using anti-CD45, anti-CD68, anti-CD3 and anti-B220 antibodies, respectively. Endothelial adherens junction was characterized using anti-Cadherin-5 (CDH5) antibodies. Edema was measured after Fibrinogen B chain (FGB) staining of muscle sections and quantified as the mean FGB-positive areas. (See Supplemental table 1 for antibody references).

Cardiomyocyte mean surface area was measured using ImageJ software after membrane staining with Wheat Germ Agglutinin (WGA), Alexa Fluor™ 488 Conjugate (Invitrogen). Fibrosis was assessed after sirius red staining of heart sections by quantifying the percentage of red stained area.

Quantifications were done on images were acquired by using an Axiozoom V16 or axioscope A1 (Zeiss) under 200x magnification. They were conducted on 10 randomly selected images were performed using ImageJ/Fiji v2.0.0-rc-59 software (National Institute of Health, USA) by an investigator blinded to genotype. More precisely, each sample received a unique number. At the end of the experiment, the genotype/treatment for each sample was revealed to enable data analysis.

For immunohistochemical analyses, primary antibodies were sequentially coupled with biotin-conjugated secondary antibodies and streptavidin-horseradish peroxidase (HRP) complex (Amersham). Staining was then revealed with a diaminobenzidine (DAB) substrate kit (Vector Laboratories) and tissue sections were counterstained with hematoxylin (see Supplemental table 2 for secondary antibody references).

For immunofluorescence analyzes, primary antibodies were resolved with Alexa-Fluor–conjugated secondary polyclonal antibodies (see Supplemental table 2). Nuclei were counterstained with DAPI (4’,6-diamidino-2-phenylindole).

For both immunohistochemical and immunofluorescence analyses, negative control experiments to check for antibody specificity were performed using secondary antibodies.

Cell culture

Human cardiac microvascular endothelial cells (HMVEC-C) (Lonza) were cultured in endothelial basal medium-2 (EBM-2) supplemented with endothelial growth medium (EGM™)-2 BulletKits™ (Lonza). Cells at passage 3 were used.

Mouse pericytes were isolated from 10 day-old pups. Briefly, hearts were dissociated using 2 mg/mL type IV collagenase (Gibco™, ThermoFisher) for 1 hour at 37°C and the resulting dissociated cells were filtrated on a 30 µm strainer. Pericytes were labelled with rat anti-mouse CD146 microbeads (Miltenyi Biotec). Labelled cells were then isolated magnetically, plated and cultured in pericyte Growth Medium 2 (PromoCell). Cells at passage 1 and 2 were used.

HMVEC-C and mouse pericytes were co-cultured in 0.4 µm-pored Transwells in 6-well plates (Corning). HMVEC-C were cultured together or not with pericytes for 24 hours.

Mouse adult cardiomyocytes were isolated: hearts were dissociated using 300 U/mL Collagenase type 2 (Worthington) via aortic catheterization and a 5-minute perfusion at 37°C. The resulting dissociated cells were then filtrated on a 400 µm mesh and centrifuged at 500 rpm for 5 minutes to

separate cardiomyocytes. Centrifuged cardiomyocytes were then incubated in increasing $CaCl_2$ concentrations (from 12,5 µmol/L to 900 µmol/L in the presence of 2 mmol/L Adenosine Triphosphate (ATP) (Sigma). Cells were centrifuged again at 500 rpm for 5 minutes, re-suspended in Minimum Essential Medium (MEM) (Gibco) containing 5% FBS, 1.26 mM $CaCl_2$, 10 mmol/L 2,3-Butanedione monoxime (Sigma) and 2 mmol/L ATP and seeded in cell culture wells coated with 10 µg/mL Laminine (Sigma). After a 2-hour incubation at 37°C, culture medium was replaced by MEM containing 0,2% bovine serum albumin (Sigma), 1.26 mM $CaCl_2$, 1X Insulin/Transferin/Selenium (Gibco) and 25 µM blebbistatin (Sigma).

Mouse cardiac pericytes were added or not to the cardiomyocytes at the same time as the change of the adhesion medium into culture medium. Cardiomyocytes were cultured together or not with pericytes for 24 hours.

Real-time quantitative polymerase chain reaction (RT-qPCR)

RNA was isolated using Tri Reagent® (Molecular Research Center Inc) as instructed by the manufacturer, from heart tissue that had been snap-frozen in liquid nitrogen and homogenized. For quantitative RT-PCR analyses, total RNA was reverse transcribed with M-MLV reverse transcriptase (Promega) and amplification was performed on an AriaMx Real Time PCR system (Agilent Technologies) using GoTaq® qPCR master mix (Promega). Primer sequences are reported in Supplementary table 3.

The relative expression of each mRNA was calculated by the comparative threshold cycle method and normalized to 18S rRNA or Actb mRNA expression.

Western blot analysis

Intercellular Adhesion Molecule 1 (ICAM1) and Vascular Cell Adhesion Molecule 1 (VCAM1) protein levels were evaluated by SDS polyacrylamide gel electrophoresis (PAGE) using goat anti-ICAM1 (R&D systems Cat# AF-796) and rabbit anti-VCAM1 (abcam, Cat# ab134047) antibodies respectively. ATPase sarcoplasmic/endoplasmic reticulum Ca2+ transporting 2 (ATP2A2) protein level was evaluated by SDS PAGE using rabbit anti-ATP2A2 antibodies (Badrilla, Cat# A010-80). Phospholamban (PLN) phosphorylation at Serine (Ser) 16 and Threonin (Thr)17 was evaluated by SDS PAGE using rabbit anti-phospho-PLN Ser16 (Badrilla, Cat# A010-12), rabbit anti-phospho-PLN Thr17 (Badrilla, Cat# A010-13) and mouse anti-total PLN (Badrilla, Cat# A010-14). Ryanodine Receptor 2 (RYR2) phosphorylation was evaluated by SDS PAGE using rabbit anti-phosphoRYR2 antibodies (Badrilla, Cat# A010-31).

Human CDH5 and ICAM1 protein levels were evaluated by SDS PAGE using rabbit anti-CDH5 (Cell signaling technology Cat# 2500) and mouse anti-ICAM1 (Santa Cruz biotechnology, Cat# sc-8439) antibodies respectively.

Protein loading quantity was controlled using mouse monoclonal anti-α-tubulin (TUB1A1) antibodies (Sigma, Cat# T5168).

Statistics

Results are reported as mean ± SEM. Comparisons between groups were analyzed for significance with the non-parametric Mann-Whitney test using GraphPad Prism v8.0.2 (GraphPad Inc, San Diego, Calif). The normality and variance were not tested. Differences between groups were considered significant when $p \leq 0.05$.

Results

Cardiac capillaries are covered by smMHC-, NG2+ pericytes

In the heart, less than 2% of vessels, essentially arterioles, are covered by smooth muscle myosin heavy chain (smMHC) positive smooth muscle cells. Indeed, the vast majorities of capillaries, i.e. 95% of them, are covered by NG2 positive, SMA negative pericytes (Figure 1A-C). Cardiac pericytes are stellate shaped cells with cytoplasmic processes contacting several capillaries (Figure 1D-F). Importantly, contrary to the brain which contains a significant amount of ensheathing and mesh pericytes [23], more than 95% of cardiac pericytes are thin-stranded pericytes (Figure S1) that do not express smMHC (Figure S2).

Pdgfrb-DTA mice display a 60% pericyte depletion in the heart

To investigate the role of cardiac pericytes, we have chosen to measure the pathophysiological consequences of partial pericyte depletion on cardiac microvasculature, cardiomyocytes, and heart function. To do so, we specifically induced diphtheria toxin A (DTA) expression under the Pdgfrb promoter in adult mice. At first, we verified that the Pdgfrb promoter was active in cardiac pericytes in adult mice, by crossing Pdgfrb-Cre/ERT2 mice with $Rosa^{mTmG}$ mice. As shown in Figure S3A-B, GFP expression, in the heart was detected in most NG2+ pericytes but also, as expected, by SMA+ smooth muscle cells.

In the meantime, we have examined GFP expression in several other organs, notably the aorta, in which GFP expression was detected in a few smooth muscle cells of the media, in the brain, in which GFP was detected in perivascular cells but also unexpectedly in glial cells, in the kidney in which GFP expression was detected in some SMA+ cells of arterioles but not in NG2 + cells within the glomerulus. Also, GFP expression was detected in capillaries within the lacteals but not in SMCs surrounding the intestine. In the lung GFP expression was detected in both arterial and capillary mural cells, however, mural cells covering lung capillaries did not express NG2. Finally in the skeletal muscle, similarly to what we found in the heart, GFP expression was detected in every pericyte and a few SMCs (Figure S4).

Pericyte depletion was then induced by tamoxifen injections in 8 week-old Pdgfrb-Cre/ERT2; Rosa-DTA mice. Notably, to maintain constant pericyte depletion in the heart over time, we had to repeat tamoxifen administrations every 2 weeks. Indeed, in mice administered with tamoxifen once during 5 consecutive days, while the percentage of NG2 positive vessels was about 20% 7 days after the first

tamoxifen injection, it was back to 90% after 28 days (Figure S5A-B) suggesting cardiac pericytes can be renewed.

After 2 series of tamoxifen injections, i.e. one month after the first one, the percentage of cardiac capillaries covered by pericytes was reduced by about 60% in Cre-positive mice compared to Cre-negative mice (Figure 1G-H), and the number of arterioles covered by SMCs reduced by about 50% (Figure 1I-J), SMC coverage of coronary arteries was sparser (Figure 1I).

In parallel, we have examined the effectiveness of mural cell depletion in other organs. The most severe phenotypes were observed in the aorta, in which the media was strongly decellularized, in the intestine lacteals, and in the skeletal muscle in which NG2+ pericytes have been fully depleted (Figure S6). These "side" depletions induced significant weight loss (Figure S7A-B) associated with circulating markers of malnutrition including decreased hemoglobin levels, triglyceride, cholesterol, and proteins levels together with decreased Aspartate aminotransferase and Alkaline phosphatase levels (Figure S7C-K). As expected, the SMC loss in the aorta decreased diastolic blood pressure. Systolic blood pressure and heart rate were not modified (Figure S7L-O). Finally, consistent with pericyte loss in the skeletal muscle, mice were severely intolerant to exercise (Figure S7P).

Altogether, these results demonstrate that Pdgfrb-DTA mice display successful pericyte-depletion in the heart. However, considering the absence of pericyte specific marker and/or the absence of cardiac mural cell-specific markers allowing pericyte-depletion in the heart only, the interpretation of the data presented in this paper may have some limitations.

Cardiac Pericyte are renewed

While performing a thorough histological analysis of the heart of Pdgfrb-DTA mice, we were surprised to see that the number of small vessels (mainly capillaries with a diameter <10 µm) covered by SMA+ cells was significantly increased in the heart of Pdgfrb-DTA mice compared to control mice (Figure 2A -B). These SMA+ cells were actually NG2 positive, suggesting that the remaining pericytes in these mice display an activated phenotype characterized by SMA expression (Figure S8A). Besides, the heart of Pdgfrb-DTA mice displayed an increased number of Vimentin (VIM) positive mesenchymal cells (Figure S8B-C). Notably, among VIM-positive cells, the number of PDGFRB negative cells (fibroblasts) did not increase (Figure S8D-E) while the number of PDGFRB positive cells significantly increased (Figure S8F). These results suggest that (1) the number of cardiac fibroblasts did not change and (2) that some pericytes expressed PDGFRB but not NG2, which we verified by doing a PDGFRB, NG2 double immunostaining (Figure 2C). Indeed, we found that, while all NG2+ pericytes expressed PDGFRB in both Pdgfrb-DTA and control mice (Figure 2D), all PDPGFRB+ pericytes did not express NG2, especially in Pdgfrb-DTA mice (Figure 2E). Considering that we found that cardiac pericytes are renewed (Figure S5), and that mice were sacrificed 10 to 13 days after the last tamoxifen injection, we believe that PDGFRB+NG2- cells are pericytes being renewed.

Consistent with the fact that the number of cardiac fibroblasts did not change, interstitial fibrosis was not significantly modulated in Pdgfrb-DTA mice; only perivascular fibrosis was (Figure S9A-C). Moreover, the expression of several markers of fibrosis including Collagen Type I Alpha 1 Chain (Col1a1), Collagen Type III Alpha 1 Chain (Col3a1), Transforming Growth Factor Beta 1 (Tgfb1), and

Connective Tissue Growth Factor (Ctgf) mRNA was not significantly different between Pdgfrb-DTA mice and control mice (Figure S9D-G).

Altogether, these results suggest that partial pericyte depletion induces activation and renewal of the remaining pericytes. Pericyte undergoing remodeling may at some points express SMA and/or PDGFRB, but not NG2.

Pericyte depletion modifies the phenotype of cardiac capillary

Then we measured the consequences of mural cell depletion on the cardiac microvasculature. As mentioned above, this was done one month after the induction of pericyte depletion. As shown in figure 3A-B, pericyte depletion did not induce microvessel rarefaction, since capillary density was equivalent in both Pdgfrb-DTA and control mice. However, pericyte depletion led to an increased capillary diameter (Figure 3C), possibly reflecting capillary disorganization, and endothelial activation characterized by a significant increase in ICAM1 and VCAM1 expression. This phenotype was attested via immunostaining (Figure 3D-E) and confirmed by western blot analyses of total heart extracts (Figure 3F-H). Also pericyte depletion led to altered endothelial intercellular junctions since we observed that CDH5 staining was discontinuous in pericyte-depleted mice (Figure 3I-J). We confirmed that endothelial intercellular junction integrity was altered in Pdgfrb-DTA mice since Fibrinogen (FGB) extravasation was significantly increased in Pdgfrb-DTA mice compared to control mice (Figure 3K-L) revealing that capillary permeability is abnormally increased in pericyte depleted mice.

To make sure these phenotypes were not due to the “unwanted” features of Pdgfrb-DTA mice such as malnutrition or decreased diastolic pressure, we confirmed the critical role of cardiac pericytes in maintaining endothelial integrity and immune quiescence in vitro. To do so, we co-cultured mouse cardiac pericytes with human microvascular cardiac ECs (HMVEC-C) (Figure S10A). HMVECs co-cultured with pericytes expressed significantly higher CDH5 protein levels, while Cadherin-2 (CDH2) mRNA was downregulated (Figure S10B-D) signing increased endothelial differentiation. Consistent with in vivo data, pericytes prevented HMVEC-C activation by decreasing ICAM1, VCAM1, and Interleukin 6 (IL-6 levels) (Figure S10E-J).

Overall, these results confirm association studies and demonstrate that pericytes are necessary for cardiac capillary integrity and immune quiescence, just as they are in the brain.

Notably, modification of the coronary vessel phenotype did not lead to cardiac hypoxia, since Hypoxia Inducible Factor 1 Subunit Alpha (HIF1A) levels were not different in the heart of Pdgfrb-DTA and control mice (Figure S11A). However, consistent with endothelial activation, Pdgfrb-DTA mice display cardiac inflammation with significantly increased Il-6 mRNA level (Figure S11B) and increased CD45+ leukocyte infiltration (Figure S11C-D) in the heart. Notably, neither CD68+ macrophage nor CD3+ T-cell infiltration was increased (Figure S11E-H), while B220+ B-cell infiltration was significantly increased (Figure S11I-J).

Pericyte depletion modifies the phenotype of cardiomyocytes

To assess the phenotype of cardiomyocytes, we first performed WGA staining on heart cross-sections and found that cardiomyocytes did not show hypertrophy (Figure 4A-B). On the contrary, Pdgfrb-DTA mice even show slight cardiac atrophy. Indeed, the heart weight over tibia length ratio tended to decrease (Figure 4C) which was confirmed by measuring the LV mass via echocardiography (Figure 4D). Consistently, cardiac wall thickness (i.e. IVS and LVPW) measured via echocardiography was thinner in Pdgfrb-DTA mice (Figure 4E-F). The LVID in diastole was not modified (Figure 4G).

Notably, WGA staining revealed that Pdgfrb-DTA had expanded cardiac interstitial space (Figure 4A), which is consistent with the increased vascular leakage.

Importantly, cardiomyocytes showed a modified phenotype with increased Myosin Heavy Chain 7 (Myh7) mRNA expression (Figure 4H) and decreased Connexin 43 (CX43) levels (Figure 4I-K). To test whether cardiomyocyte contractility could be affected by pericyte depletion, we measured expression and/or phosphorylation of proteins regulating calcium homeostasis. We first measured ATPase Sarcoplasmic/Endoplasmic Reticulum Ca2+ Transporting 2 (ATP2A2) expression and found it significantly downregulated at both mRNA and protein levels in Pdgfrb-DTA mice compared to control mice (Figure 5A-C). This was associated with diminished Phospholamban (PLN) phosphorylation at both Serine 16 and Threonine 17. (Figure 5D-F). On the contrary, Ryanodine Receptor 2 (RYR2) phosphorylation at serine 2814 was not significantly different in both groups (Figure 5G-H). To assess cardiomyocyte stiffness, we quantified the mRNA expression of each Titin (Ttn) isoform. Expression of stiff Ttn isoform N2B was significantly diminished while expression of Ttn N2BA isoform tended to increase. Accordingly, the N2BA/N2B ratio was significantly increased (Figure 5I-K).

Altogether these results demonstrate that pericyte depletion modifies the phenotype of cardiomyocytes which displays a Titin isoform ratio consistent with heart failure in humans [24].

Once again, in order to make sure these changes in the phenotype of cardiomyocytes were not due to the “unwanted” features of Pdgfrb-DTA mice such as malnutrition or decreased diastolic pressure, we performed co-culture assays. More specifically, mouse adult cardiomyocytes were co-cultured or not with mouse cardiac pericytes (Figure S12A). While the presence of pericytes did not modify Atp2a2 or Myh7 mRNA expression in cardiomyocytes (Figure S12B-C), it did significantly increase Cx43 mRNA expression (Figure S12D) demonstrating for the first time that cardiac pericytes may modify the phenotype of cardiomyocytes directly. Besides, we found that pericytes have an anti-inflammatory effect on cardiomyocytes like they have on ECs by downregulating Il-6 mRNA expression (Figure S12E).

In order to test whether cardiac inflammation (i.e. Il-6 overexpression) may indirectly also affect cardiomyocytes, mouse adult cardiomyocytes were treated or not with recombinant IL-6. We found that IL-6 did not modulate Cx43 or Myh7 mRNA expression. However, it significantly downregulated Atp2a2 mRNA expression.

Altogether these results demonstrate that cardiac pericytes may affect the phenotype of cardiomyocytes directly, notably by upregulating CX43 and downregulating IL-6. The increased

cardiac inflammation secondary to pericyte depletion is likely responsible for the decreased Atp2a2 mRNA expression observed in the heart of Pdgfrb-DTA mice. However, the mechanism leading to the increased Myh7 mRNA expression remains to be identified.

Pericyte depletion impairs both systolic and diastolic function

Finally, to test whether pericyte depletion and the associated cardiac remodeling result in cardiac dysfunction, we performed an echocardiography and left ventricular catheterization. As shown in figure 6, LVEF was significantly reduced in Pdgfrb-DTA mice indicating systolic dysfunction (Figure 6A). LVEF was positively correlated with pericyte coverage (Figure 6B). Consistent with systolic dysfunction, cardiac contractility (attested by dP/dt max and contractility index) significantly decreased (Figure 6C-E) while LV end-systolic volume significantly increased (Figure 6F-G) in pericyte depleted mice compared to control mice.

Mice depleted from cardiac pericytes also displayed diastolic dysfunction attested by increased end diastolic pressure (EDP) (Figure 6H,I) and decreased dP/dt min (Figure 6J-K). Relaxation constant Tau tended to increase in Pdgfrb-DTA mice but the difference did not reach significance (Figure 6L).

In conclusion, this study demonstrates for the first time that pericytes are necessary for proper cardiac function possibly by affecting the phenotype of cardiomyocytes directly.

Discussion

The present study demonstrates for the first time that, just like in the brain, pericytes are necessary for endothelium integrity and immune quiescence in the heart. Importantly, in this organ, pericytes are not only necessary for coronary vasculature integrity but also for proper cardiac function suggesting that modifications of pericyte properties may participate in the pathophysiology of cardiac diseases.

Besides, this study reveals that cardiac pericytes may undergo strong remodeling upon injury (e.i. renewal, expression of SMA). This is consistent with what has been observed in obese and hypertensive ZSF1rats [15] in which pericytes were shown to be disorganized and more numerous. This piece of data actually suggests that, even though pericytes may induce similar effects in the brain and in the heart by maintaining microvasculature integrity, pericyte turnover and biology in these organs may be very different. Indeed, in the central nervous system, pericyte impairment seems to be essentially characterized by pericyte loss. Notably, one of the earliest hallmarks of diabetic retinopathy is the loss of pericytes. The diabetic microenvironment is suggested to be particularly detrimental to pericyte survival in the retina since during the early stages of retinopathy, the pericyte to EC ratio decreases from 1:1 to 1:4 [25]. In the brain, pericyte number and coverage in the cortex and hippocampus of subjects with Alzheimer's disease compared with neurologically intact controls were shown to be reduced by 59% and 60% [26]. Similarly, in the spinal cord, immunostaining for PDGFRB, has indicated a 54 % ($p < 0.01$) reduction in the number of pericytes in amyotrophic lateral sclerosis patients compared to control patients [27]. However, in the heart, pericyte impairment is more likely characterized by phenotypic changes with the acquisition of an ‘activated’ phenotype. Notably, the

number of pericytes was shown to increase in the heart of mice infused with angiotensin-2. Moreover, these pericytes express higher levels of SMA [28]. As mentioned above, cardiac pericytes were shown to be disorganized and more numerous in obese and hypertensive ZSF1 rats (van Dijk et al. 2016). In our model, pericyte depletion induced pericyte activation and renewal.

Pericyte loss has been previously associated with reduced LVEF (Chintalgattu et al. 2013) (He, Zeng, and Chen 2016), dilated cardiomyopathy, cardiac fibrosis, contractile dysfunction (Siao et al. 2012), and cardiac hypertrophy (Tao et al. 2017). Our study confirms that pericytes are necessary for proper cardiac contractility and systolic function, while pericyte loss does not seem to promote cardiac fibrosis, hypertrophy, or dilation. In Siao et al. study, cardiac fibrosis, and dilation may then be due to the effect of the mutant form of ProNGF on other cell types, notably cardiomyocytes and/or fibroblasts (Siao et al. 2012), while in Tao et al. study (Tao et al. 2017), cardiac hypertrophy may be due to Notch3 deletion in cardiomyocytes [29].

Importantly, this study suggests that pericytes may modify the phenotype of cardiomyocytes directly, notably by upregulating Cx43 and downregulating Il-6. Another study has also suggested that pericytes may dialogue with cardiomyocytes directly via MiR-132 transfer [30].

One of the main limitations of this study is technical because a mouse model only targeting cardiac pericytes still needs to be generated to obtain robust and specific characterization of the role of cardiac pericytes. Indeed, the Pdgfrb promoter does not only target pericytes but also SMCs and the Pdgfrb promoter does not only target cardiac mural cells but mural cells of the entire body. However, several mouse models targeting pericytes have been used especially in the brain and most of these models are based on PDGFB-PDGFRB signaling which is crucial for pericyte recruitment and survival [31]. At first, developmental studies were performed on *Pdgfb* [32] and *Pdgfrb* [33] deficient embryos, which are not viable. Then mice harboring mutations within the *Pdgfrb* gene (the *Pdgfrb*$^{redeye/redeye}$ mutant [34] and the *Pdgfrb*$^{F7/F7}$ mutant [35]) were used. These mutants display progressive pericyte loss, especially in the central nervous system (brain and retina). Mouse models with inducible pericyte depletion have been developed. These models are tamoxifen-inducible, and use either Diphtheria toxin A (DTA) or its receptor Diphtheria toxin receptor (DTR) to induce cell ablation [36]. These last models allow the exploration of the role of pericytes in adults excluding the potential consequences of developmental defects. The Pdgfrb-Cre/ERT2; Rosa iDTR model is proposed to induce a less severe pericyte depletion than the Pdgfrb-Cre/ERT2; Rosa iDTA model however, it requires administration of both tamoxifen and Diphtheria toxin [36]. Alternatively to the *Pdgfrb* promoter, the *Cspg4* (also known as NG2) promoter has been proposed to induce pericyte depletion. However, its induction efficiency is lower than the one of Pdgfrb, and just like the Pdgfrb promoter, it induces recombination in SMCs [37]. Finally, a strategy utilizing a double-promoter approach with Pdgfrb and the Cspg4 has been used [38] to target pericytes more specifically, but both promoters also target SMCs as described above. Cell culture assays, have also limitations, however, they may help demonstrating pericyte specific effects.

In conclusion, the present study highlights the critical role of pericytes in the heart. Just like in the brain, cardiac pericytes are necessary to maintain coronary vasculature integrity and immune quiescence. Importantly, cardiac pericytes may protect from cardiac inflammation, not only by acting on ECs, but also by downregulating Il-6 mRNA expression in cardiomyocytes. Finally, cardiac pericytes increase Cx43 mRNA expression in cardiomyocytes suggesting they may directly participate in the

regulation of cardiac function. Altogether, these results demonstrate that the role of cardiac pericytes should be considered when investigating the pathophysiology of cardiac diseases.

Acknowledgments

We thank Annabel Reynaud, Sylvain Grolleau, and Maxime David for their technical help.

Sources of funding

This study was supported by grants from the Fondation pour la Recherche Médicale (équipe FRM), and the Agence Nationale pour la Recherche (Appel à Projet Générique). Additionally, this study was co-funded by the "*Institut National de la Santé et de la Recherche Médicale*" (Inserm), and by the University of Bordeaux. Lauriane Cornuault received a fellowship from the Fondation pour la Recherche Médicale. François-Xavier Hérion received a fellowship from Bordeaux university hopital.

Conflict of Interest Disclosures

none

References

1. Armulik A, Abramsson A, Betsholtz C. Endothelial/pericyte interactions. *Circ Res*. 2005;97:512–523.

2. Armulik A, Genové G, Mäe M, Nisancioglu MH, Wallgard E, Niaudet C, He L, Norlin J, Lindblom P, Strittmatter K et al. Pericytes regulate the blood–brain barrier. *Nature*. 2010;468:557–561.

3. Daneman R, Zhou L, Kebede AA, Barres BA. Pericytes are required for blood-brain barrier integrity during embryogenesis. *Nature*. 2010;468:562–566.

4. Vazquez-Liebanas E, Nahar K, Bertuzzi G, Keller A, Betsholtz C, Mäe MA. Adult-induced genetic ablation distinguishes PDGFB roles in blood-brain barrier maintenance and development. *J Cereb Blood Flow Metab*. 2022;42:264–279.

5. Su H, Cantrell AC, Zeng H, Zhu S-H, Chen J-X. Emerging Role of Pericytes and Their Secretome in the Heart. *Cells*. 2021;10:548.

6. Chintalgattu V, Rees ML, Culver JC, Goel A, Jiffar T, Zhang J, Dunner K, Pati S, Bankson JA, Pasqualini R et al. Coronary microvascular pericytes are the cellular target of sunitinib malate-induced cardiotoxicity. *Sci Transl Med*. 2013;5:187ra69.

7. Siao C-J, Lorentz CU, Kermani P, Marinic T, Carter J, McGrath K, Padow VA, Mark W, Falcone DJ, Cohen-Gould L et al. ProNGF, a cytokine induced after myocardial infarction in humans, targets pericytes to promote microvascular damage and activation. *J Exp Med*. 2012;209:2291–2305.

8. He X, Zeng H, Chen J-X. Ablation of SIRT3 Causes Coronary Microvascular Dysfunction and Impairs Cardiac Recovery Post Myocardial Ischemia. *Int J Cardiol*. 2016;215:349–357.

9. Tao Y-K, Zeng H, Zhang G-Q, Chen ST, Xie X-J, He X, Wang S, Wen H, Chen J-X. Notch3 deficiency impairs coronary microvascular maturation and reduces cardiac recovery after myocardial ischemia. *Int J Cardiol*. 2017;236:413–422.

10. Greenhalgh SN, Iredale JP, Henderson NC. Origins of fibrosis: pericytes take centre stage. *F1000Prime Rep*. 2013;5:37.

11. O'Farrell FM, Mastitskaya S, Hammond-Haley M, Freitas F, Wah WR, Attwell D. Capillary pericytes mediate coronary no-reflow after myocardial ischaemia. *Elife*. 2017;6:e29280.

12. Methner C, Cao Z, Mishra A, Kaul S. Mechanism and potential treatment of the "no reflow" phenomenon after acute myocardial infarction: role of pericytes and GPR39. *Am J Physiol Heart Circ Physiol*. 2021;321:H1030–H1041.

13. Chen J, Sivan U, Tan SL, Lippo L, De Angelis J, Labella R, Singh A, Chatzis A, Cheuk S, Medhghalchi M et al. High-resolution 3D imaging uncovers organ-specific vascular control of tissue aging. *Sci Adv*. 2021;7. doi:10.1126/sciadv.abd7819.

14. Zeng H, Vaka VR, He X, Booz GW, Chen J-X. High-fat diet induces cardiac remodelling and dysfunction: assessment of the role played by SIRT3 loss. *J Cell Mol Med*. 2015;19:1847–1856.

15. van Dijk CGM, Oosterhuis NR, Xu YJ, Brandt M, Paulus WJ, van Heerebeek L, Duncker DJ, Verhaar MC, Fontoura D, Lourenço AP et al. Distinct Endothelial Cell Responses in the Heart and Kidney Microvasculature Characterize the Progression of Heart Failure With Preserved Ejection Fraction in the Obese ZSF1 Rat With Cardiorenal Metabolic Syndrome. *Circulation: Heart Failure*. 2016;9:e002760.

16. Robinson FA, Mihealsick RyanP, Wagener BM, Hanna P, Poston MD, Efimov IR, Shivkumar K, Hoover DB. Role of angiotensin-converting enzyme 2 and pericytes in cardiac complications of COVID-19 infection. *Am J Physiol Heart Circ Physiol*. 2020;319:H1059–H1068.

17. Bischoff FC, Werner A, John D, Boeckel J-N, Melissari M-T, Grote P, Glaser SF, Demolli S, Uchida S, Michalik KM et al. Identification and Functional Characterization of Hypoxia-Induced Endoplasmic Reticulum Stress Regulating lncRNA (HypERlnc) in Pericytes. *Circ Res*. 2017;121:368–375.

18. Percie du Sert N, Hurst V, Ahluwalia A, Alam S, Avey MT, Baker M, Browne WJ, Clark A, Cuthill IC, Dirnagl U et al. The ARRIVE guidelines 2.0: Updated guidelines for reporting animal research. *Br J Pharmacol*. 2020;177:3617–3624.

19. Renault MA, Roncalli J, Tongers J, Misener S, Thorne T, Jujo K, Ito A, Clarke T, Fung C, Millay M et al. The Hedgehog transcription factor Gli3 modulates angiogenesis. *Circ Res*. 2009;105:818–26.

20. Roncalli J, Renault MA, Tongers J, Misener S, Thorne T, Kamide C, Jujo K, Tanaka T, Ii M, Klyachko E et al. Sonic hedgehog-induced functional recovery after myocardial infarction is enhanced by AMD3100-mediated progenitor-cell mobilization. *J Am Coll Cardiol*. 2011;57:2444–52.

21. Schiller NB, Shah PM, Crawford M, DeMaria A, Devereux R, Feigenbaum H, Gutgesell H, Reichek N, Sahn D, Schnittger I. Recommendations for quantitation of the left ventricle by two-dimensional echocardiography. American Society of Echocardiography Committee on Standards,

Subcommittee on Quantitation of Two-Dimensional Echocardiograms. *J Am Soc Echocardiogr*. 1989;2:358–367.

22. Mohan JC, Sethi KK, Arora R, Khalilullah M. Cross sectional echocardiographic left ventricular ejection fraction: method based variability. *Indian Heart J*. 1992;44:23–28.

23. Abdelazim H, Payne LB, Nolan K, Paralkar K, Bradley V, Kanodia R, Gude R, Ward R, Monavarfeshani A, Fox MA et al. Pericyte heterogeneity identified by 3D ultrastructural analysis of the microvessel wall. *Front Physiol*. 2022;13:1016382.

24. Borbély A, Falcao-Pires I, van Heerebeek L, Hamdani N, Edes I, Gavina C, Leite-Moreira AF, Bronzwaer JGF, Papp Z, van der Velden J et al. Hypophosphorylation of the Stiff N2B titin isoform raises cardiomyocyte resting tension in failing human myocardium. *Circ Res*. 2009;104:780–786.

25. Robison WG, Kador PF, Kinoshita JH. Early retinal microangiopathy: prevention with aldose reductase inhibitors. *Diabet Med*. 1985;2:196–199.

26. Sengillo JD, Winkler EA, Walker CT, Sullivan JS, Johnson M, Zlokovic BV. Deficiency in mural vascular cells coincides with blood-brain barrier disruption in Alzheimer's disease. *Brain Pathol*. 2013;23:303–310.

27. Winkler EA, Sengillo JD, Sullivan JS, Henkel JS, Appel SH, Zlokovic BV. Blood-spinal cord barrier breakdown and pericyte reductions in amyotrophic lateral sclerosis. *Acta Neuropathol*. 2013;125:111–120.

28. Su H, Zeng H, Liu B, Chen J. Sirtuin 3 is essential for hypertension-induced cardiac fibrosis via mediating pericyte transition. *J Cell Mol Med*. 2020;24:8057–8068.

29. Øie E, Sandberg WJ, Ahmed MS, Yndestad A, Lærum OD, Attramadal H, Aukrust P, Eiken HG. Activation of Notch signaling in cardiomyocytes during post-infarction remodeling. *Scand Cardiovasc J*. 2010;44:359–366.

30. Katare R, Riu F, Mitchell K, Gubernator M, Campagnolo P, Cui Y, Fortunato O, Avolio E, Cesselli D, Beltrami AP et al. Transplantation of Human Pericyte Progenitor Cells Improves the Repair of Infarcted Heart Through Activation of an Angiogenic Program Involving Micro-RNA-132. *Circ Res*. 2011;109:894–906.

31. Hoch RV, Soriano P. Roles of PDGF in animal development. *Development*. 2003;130:4769–4784.

32. Levéen P, Pekny M, Gebre-Medhin S, Swolin B, Larsson E, Betsholtz C. Mice deficient for PDGF B show renal, cardiovascular, and hematological abnormalities. *Genes Dev*. 1994;8:1875–1887.

33. Soriano P. Abnormal kidney development and hematological disorders in PDGF beta-receptor mutant mice. *Genes Dev*. 1994;8:1888–1896.

34. Jadeja S, Mort RL, Keighren M, Hart AW, Joynson R, Wells S, Potter PK, Jackson IJ. A CNS-Specific Hypomorphic Pdgfr-Beta Mutant Model of Diabetic Retinopathy. *Invest Ophthalmol Vis Sci*. 2013;54:3569–3578.

35. Nikolakopoulou AM, Zhao Z, Montagne A, Zlokovic BV. Regional early and progressive loss of brain pericytes but not vascular smooth muscle cells in adult mice with disrupted platelet-derived growth factor receptor-β signaling. *PLoS One*. 2017;12:e0176225.

36. Eilken HM, Diéguez-Hurtado R, Schmidt I, Nakayama M, Jeong H-W, Arf H, Adams S, Ferrara N, Adams RH. Pericytes regulate VEGF-induced endothelial sprouting through VEGFR1. *Nat Commun*. 2017;8:1574.

37. Mayr D, Preishuber-Pflügl J, Koller A, Brunner SM, Runge C, Ladek A-M, Rivera FJ, Reitsamer HA, Trost A. Characterization of the Two Inducible Cre Recombinase-Based Mouse Models NG2-CreER^{TM} and PDGFRb-P2A-CreERT2 for Pericyte Labeling in the Retina. *Curr Eye Res*. 2022;:1–7.

38. Nikolakopoulou AM, Montagne A, Kisler K, Dai Z, Wang Y, Huuskonen MT, Sagare AP, Lazic D, Sweeney MD, Kong P, Wang M et al. Pericyte loss leads to circulatory failure and pleiotrophin depletion causing neuron loss. *Nat Neurosci*. 2019;22:1089–1098.

Figures and Figure legends

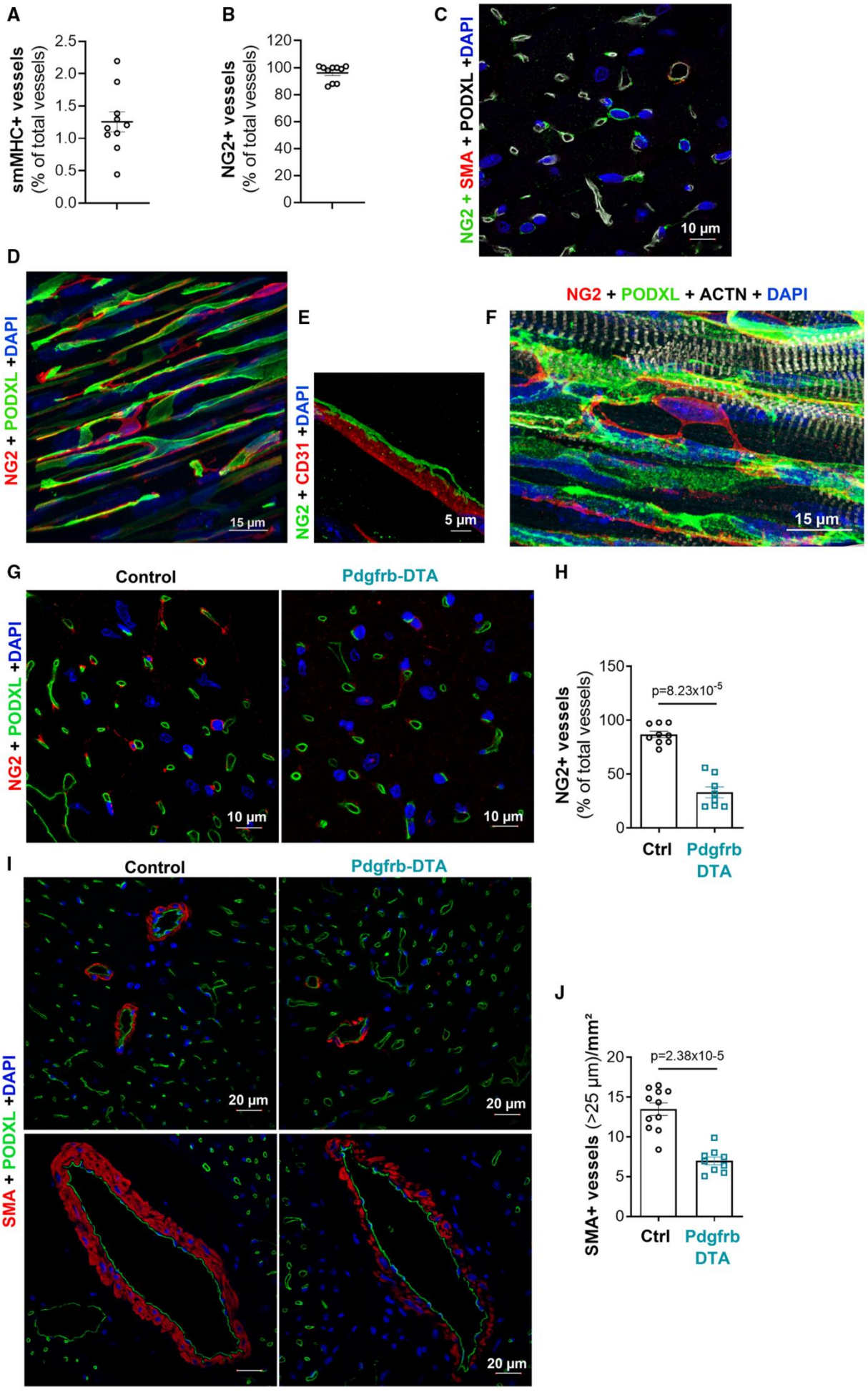
A
smMHC+ vessels
(% of total vessels)
2.5
2.0
1.5
1.0
0.5
0.0
B
NG2+ vessels
(% of total vessels)
120
100
80
60
40
20
0
C
NG2 + SMA + PODXL +DAPI
10 µm
D
NG2 + PODXL +DAPI
15 µm
E
NG2 + CD31 +DAPI
5 µm
F
NG2 + PODXL + ACTN + DAPI
15 µm
G
Control
Pdgfrb-DTA
NG2 + PODXL +DAPI
10 µm
10 µm
H
NG2+ vessels
(% of total vessels)
150
100
50
0
p=8.23x10-5
Ctrl
Pdgfrb DTA
I
Control
Pdgfrb-DTA
SMA + PODXL +DAPI
20 µm
20 µm
20 µm
J
SMA+ vessels (>25 µm)/mm²
20
15
10
5
0
p=2.38x10-5
Ctrl
Pdgfrb DTA

Figure 1: 95 % of the cardiac vasculature is covered by pericytes. (A) Heart cross-sections were co-immunostained with anti-smMHC and anti-PODXL antibodies to identify SMCs and ECs respectively. The percentage of smMHC+ vessels over total PODXL+ vessels was calculated. **(B)** Heart cross-sections were co-immunostained with anti-NG2 and anti-PODXL antibodies to identify pericytes and ECs respectively. The percentage of NG2+ vessels over total PODXL+ vessels was calculated. (**C**) Heart cross-section were co-immunostained with anti-SMA (in red), anti-NG2 (in green), and anti-PODXL (in white) antibodies to identify SMCs, pericytes and ECs respectively. (**D**) Heart thick sections were co-immunostained with anti-NG2 (in red) and anti-PODXL (in green) antibodies to identify pericytes, and ECs respectively. (**E**) Heart thick sections were co-immunostained with anti-NG2 (in green) and anti-CD31 (in red) antibodies to identify pericytes and ECs respectively. (**F**) Heart thick sections were co-immunostained with anti-NG2 (in red), anti-PODXL (in green), and anti-ACTN2 (in white) antibodies to identify pericytes, ECs, and cardiomyocytes respectively. (**G-J**) Pdgfrb-Cre/ERT2; $Rosa^{DTA}$ (Pdgfrb-DTA) and $Rosa^{DTA}$ (Control) mice were administered with tamoxifen. Mice were sacrificed 28 days after the first injection. (**G**) Heart cross-sections were co-immunostained with anti-NG2 (in red) and anti-PODXL (in green) antibodies to identify pericytes and ECs respectively. (**H**) The percentage of NG2+ vessels over total PODXL+ vessels was calculated (n=8 and 9 mice/group). (**I**) Heart cross-sections were co-immunostained with anti-SMA (in red) and anti-PODXL (in green) antibodies to identify SMCs and ECs respectively. (**J**) The number of SMA+ vessels per mm^2 was counted (n=9 and 11 mice per group). Mann Whitney tests

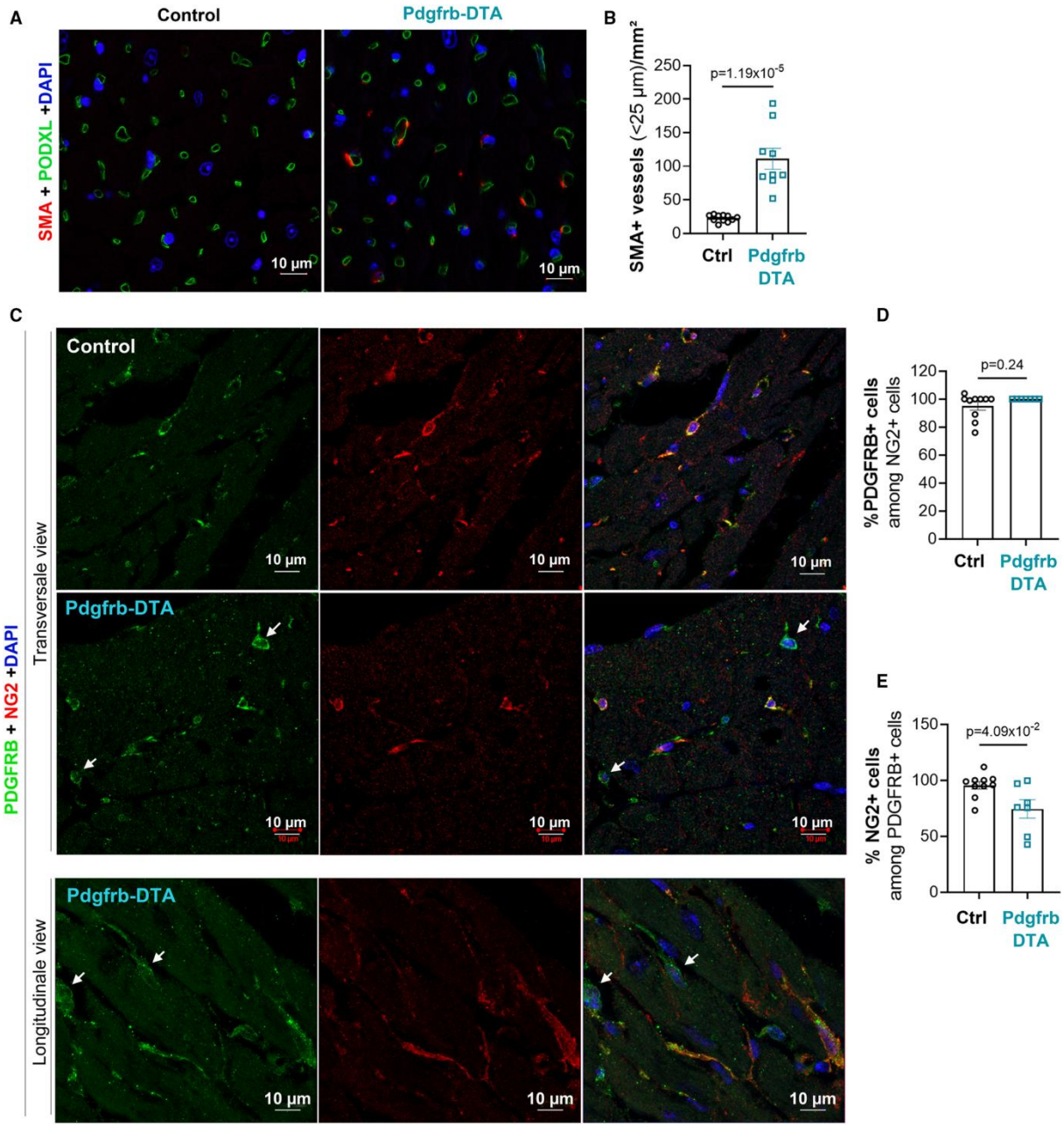

Figure 2: Cardiac pericytes may undergo strong remodeling. Pdgfrb-Cre/ERT2; Rosa^{DTA} (Pdgfrb-DTA) and Rosa^{DTA} (Control) mice were administered with tamoxifen. Mice were sacrificed 28 days after the first injection. (**A**) Heart cross sections were co-immunostained with anti-SMA (in red) and anti-PODXL (in green) antibodies to identify SMCs and ECs respectively. (**B**) The number of SMA+ vessels with a diameter ≤25 µm per mm² was counted (n=9 and 11 mice per group). (**C**) Heart cross sections were co-immunostained with anti-PDGFRB (in green), anti-NG2 (in red) antibodies. (**D**) The percentage of PDGFRB+ cells among NG2+ cells was calculated (n=7 and 10 mice per group). (**E**) The percentage of NG2+ cells among PDGFRB+ cells was calculated (n=7 and 10 mice per group). Mann Whitney tests

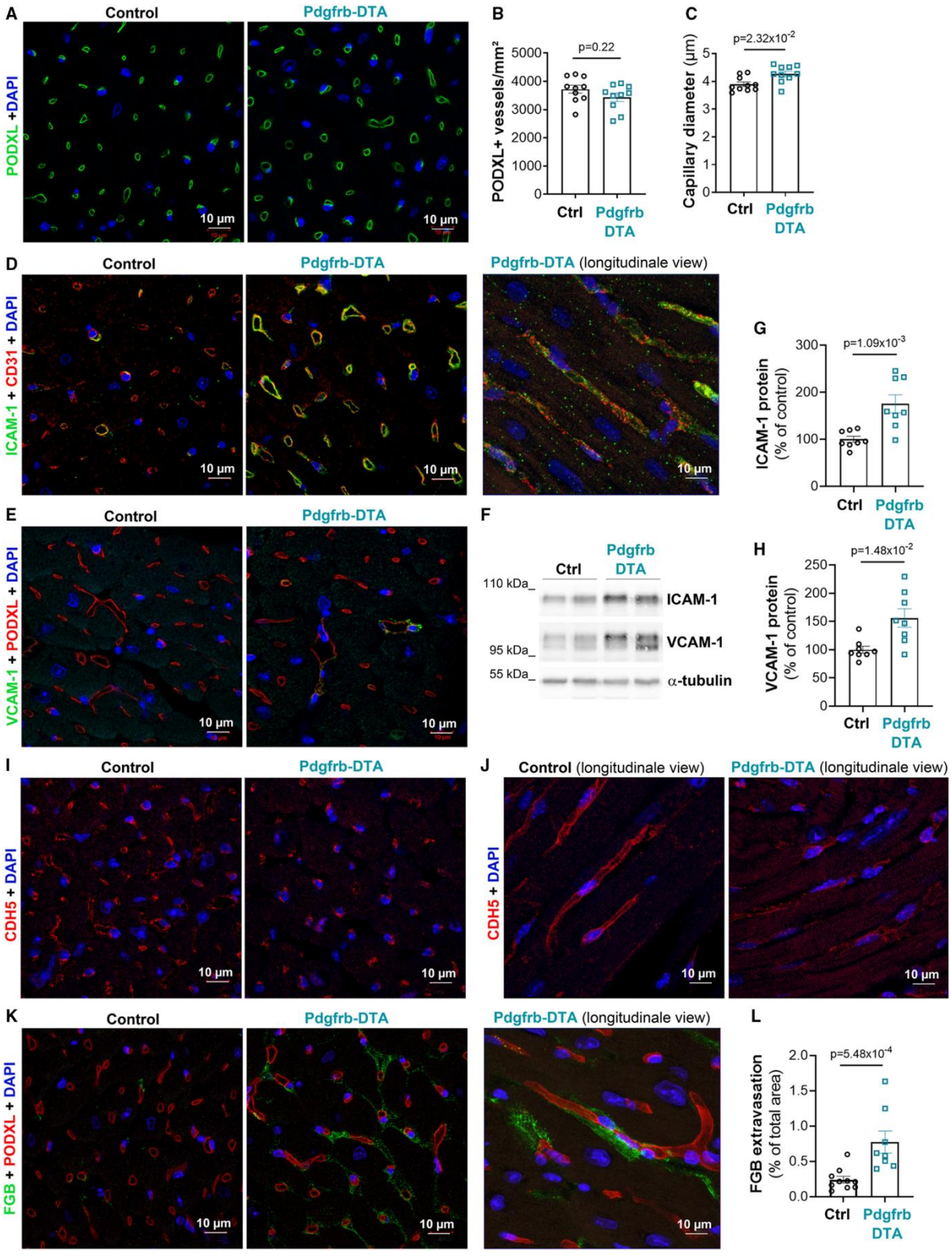

Figure 3: Pericyte are necessary to maintain cardiac capillary integrity. Pdgfrb-Cre/ERT2; Rosa^{DTA} (Pdgfrb-DTA) and Rosa^{DTA} (Control) mice were administered with tamoxifen. Mice were sacrificed 28 days after the first injection. (**A**) Heart cross sections were immunostained with anti-PODXL antibodies to identify ECs. (**B**) The number of PODXL+ capillary per mm² was counted (n=14 and 11 mice per group). (**C**) the mean capillary diameter was measured (n=10 mice in each group) (**D**) Heart cross sections were co-immunostained with anti-ICAM-1 (in green) and anti-CD31 (in red) antibodies.

(**E**) Heart cross sections were co-immunostained with anti-VCAM-1 (in green) and anti-PODXL (in red) antibodies. (**F**) ICAM1 and VCAM1 protein expression was evaluated in total heart extract by western blot analyses. ICAM1 (**G**) and VCAM1 (**H**) protein was quantified using image J software and normalized to α-tubulin (n=8 mice per group). (**I-J**) Heart cross sections were immunostained with anti-CDH5 antibodies to identify adherens junction. (**K**) Heart cross sections were co-immunostained with anti-FGB and anti-PODXL antibodies. (**L**) FGB+ surface area was measured using Image J software (n=10 and 8 mice per group). Mann Whitney tests

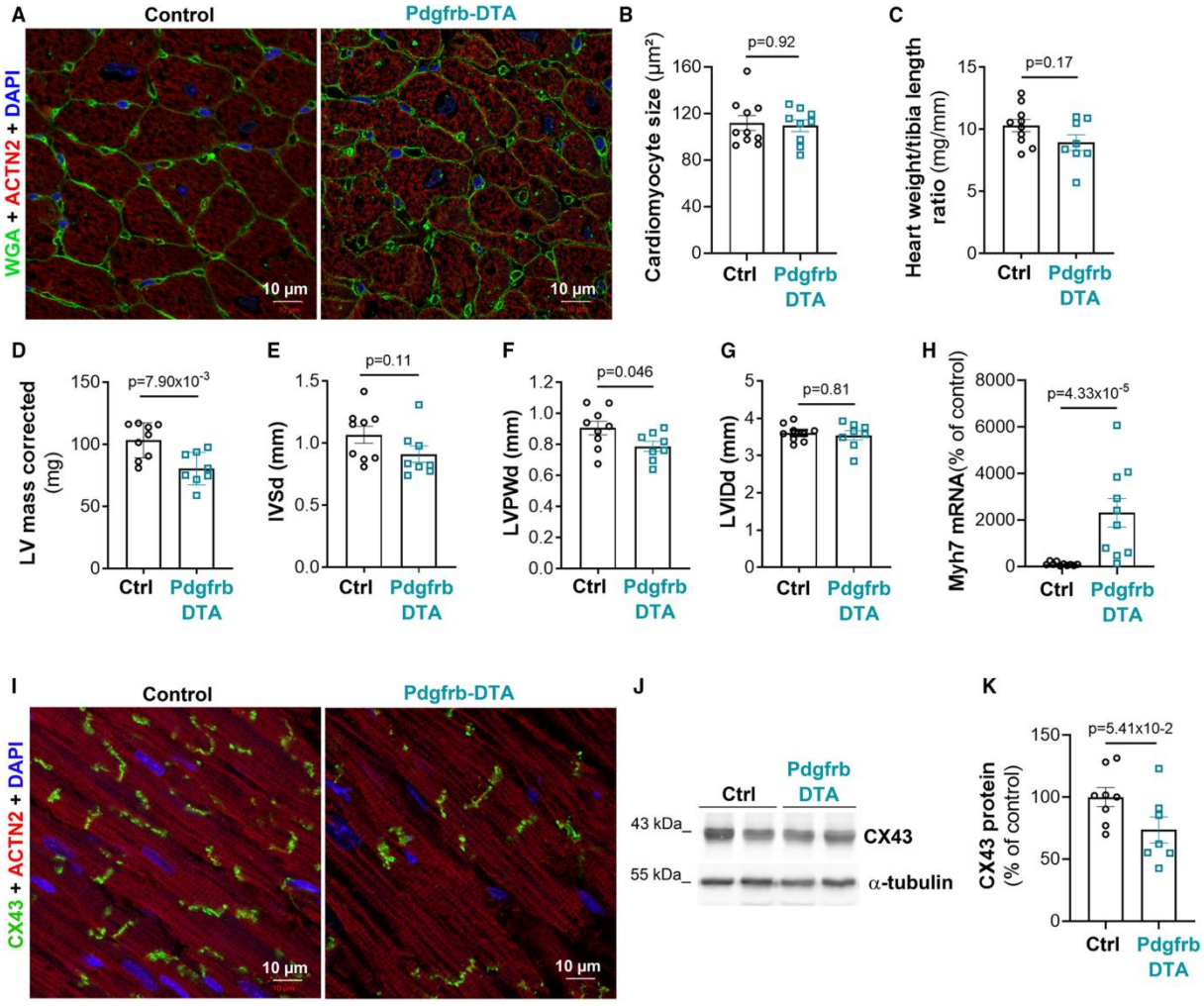

Figure 4: Pericyte depletion induces cardiomyocyte dedifferentiation but not cardiomyocyte hypertrophy. Pdgfrb-Cre/ERT2; Rosa^{DTA} (Pdgfrb-DTA) and Rosa^{DTA} (Control) mice were administered with tamoxifen. Mice were sacrificed 28 days after the first injection. (**A**) Heart cross sections were co-stained with WGA (in green) and anti-ACTN2 (in red) antibodies. (**B**) Cardiomyocyte cross section area was measured using Image J software (n=11 and 9 mice per group). (**C**) The heart weight over tibia length was measured (n=10 and 8 mice per group). (**D**) The LV mass corrected was measured via echocardiography. IVS thickness (**E**), LVPW thickness (**F**) and left ventricular internal diameter (**G**) were measured by echocardiography in diastole. (**H**) Myh7 mRNA expression was quantified by RT-qPCR in total heart extract and normalized to 18S rRNA (n= 9 and 10 mice per group). (**I**) Heart cross sections were co-immunostained with anti-CX43 (in green) and anti-ACTN2 (in red) antibodies. (**J**) CX43 protein expression was analyzed by western blot and (**K**) quantified using Image J software (n=7 and 8 mice per group). Mann Whitney tests

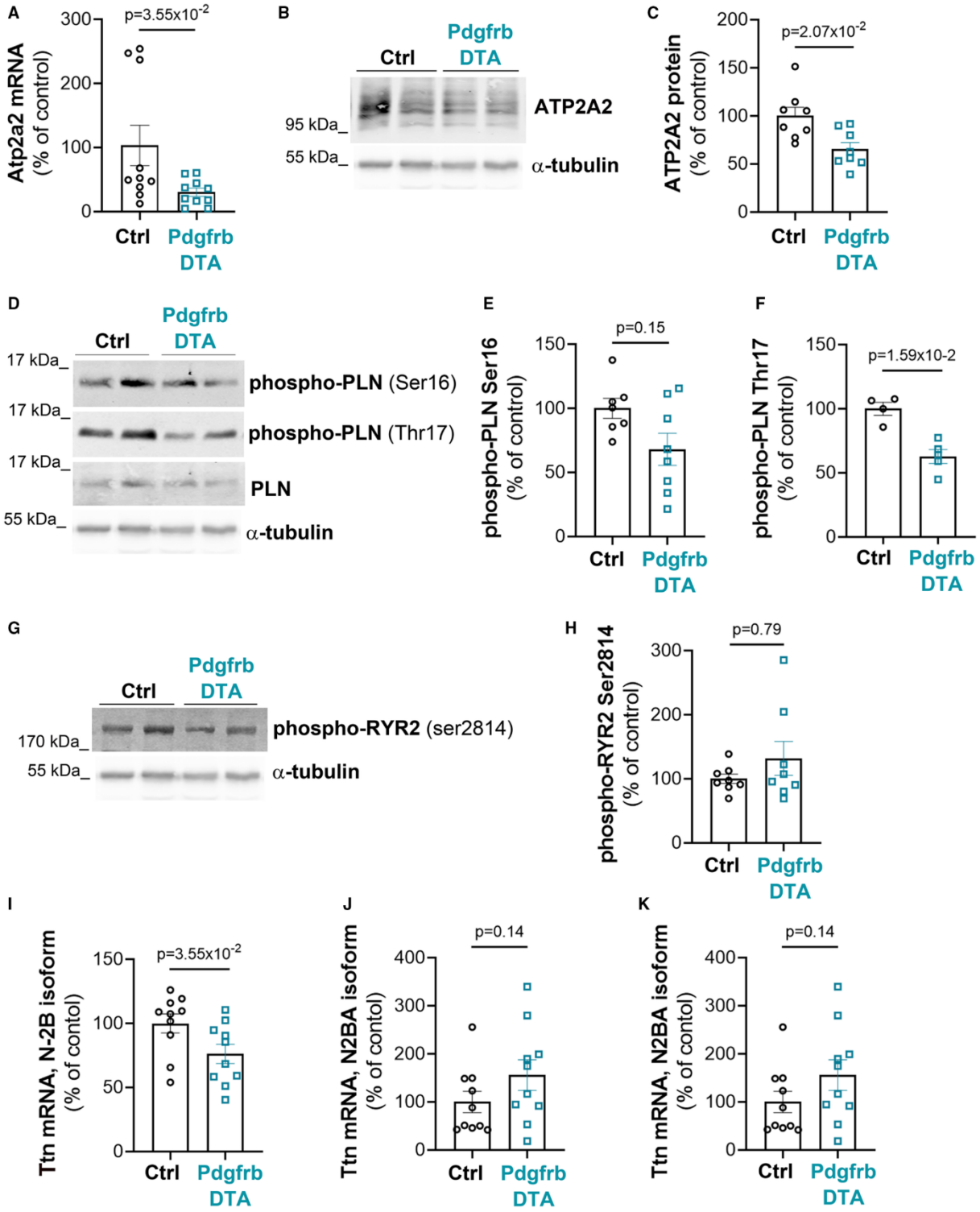

Figure 5: Pericyte depletion modifies ATP2A2 level and Ttn splicing in cardiomyocytes. Pdgfrb-Cre/ERT2; Rosa^{DTA} (Pdgfrb-DTA) and Rosa^{DTA} (Control) mice were administered with tamoxifen. Mice were sacrificed 28 days after the first injection. (**A**) Atp2a2 mRNA expression was quantified by RT-qPCR in total heart extract and normalized to 18S rRNA (n=10 mice in each group). (**B**) ATP2A2 protein expression was analysed by western blot in total heart extract and (**C**) quantified using Image J software (n=8 mice in each group). (**D**) PLN phosphorylation was assessed by western blot analyses and (**E,F**) quantified using Image J software (n=5 to 8 mice per group). (**G**) RYR2 phosphorylation was assessed by western blot analyses and (**H**) quantified using Image J software (n=8 mice in each

group). Ttn, isoform N-2B (**I**) and N2BA (J) mRNA expression was quantified by RT-qPCR in total heart extract and normalized to 18S rRNA (n=10 mice in each group). (**K**) N2BA mRNA/N2B mRNA ratio was calculated. Mann Whitney tests

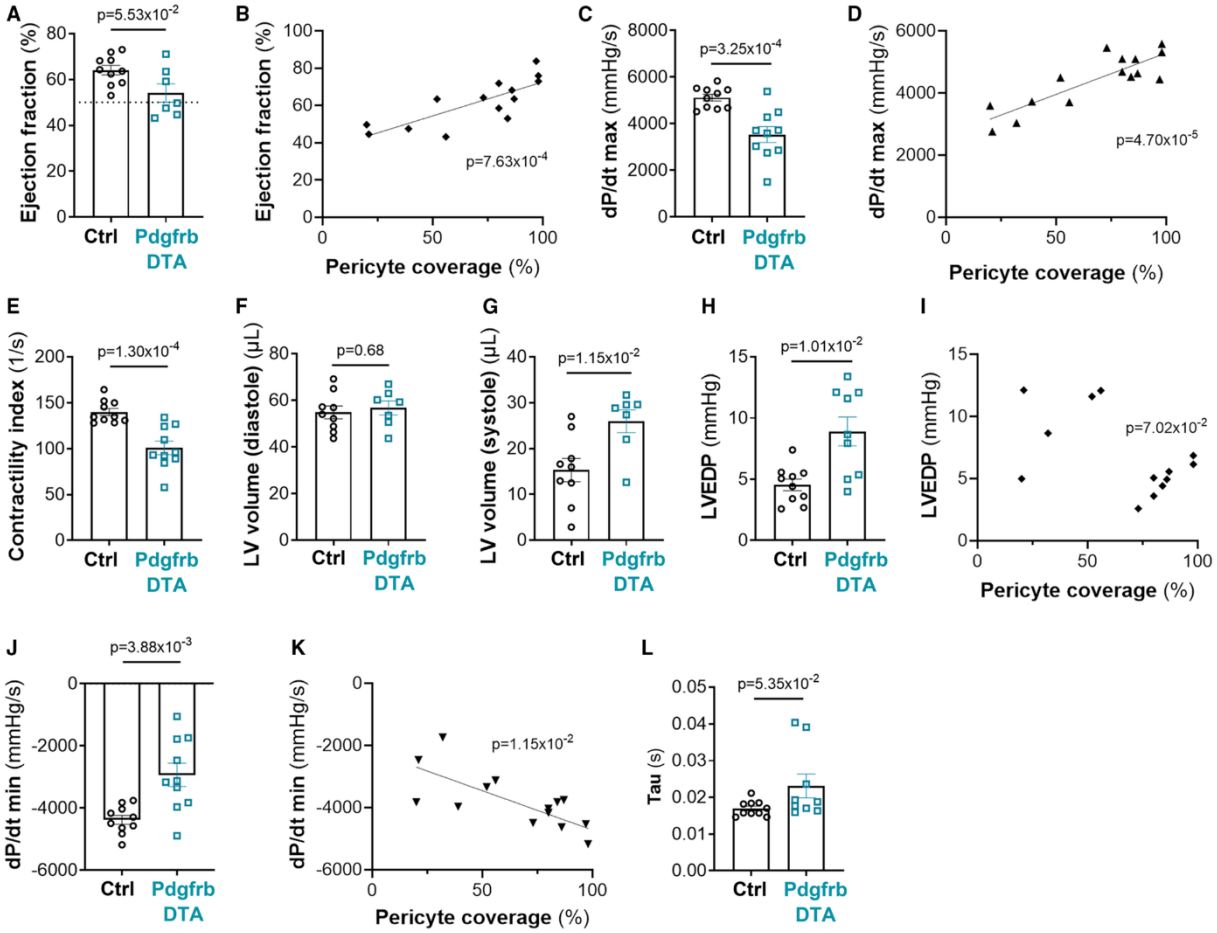

Figure 6: Pericyte depletion induces both systolic and diastolic dysfunction. Pdgfrb-Cre/ERT2; Rosa^{DTA} (Pdgfrb-DTA) and Rosa^{DTA} (Control) mice were administered with tamoxifen. Mice were sacrificed 28 days after the first injection. (**A**) LVEF was assessed via echocardiography (n=7 and 10) and (**B**) correlated with pericyte coverage. (**C**) dP/dt max was measured by left ventricular catheterization (n=10 in each group), and (**D**) correlated with pericyte coverage. **(E**) The contractility index was measured by left ventricular catheterization (n=10 mice in each group). LV volumes were measured in diastole (**F**) and systole (**G**) via echocardiography (n=7 and 10 mice per group). (**H** LV end-diastolic pressure (EDP) was measured by left ventricular catheterization (n=10 mice in each group) (**I**) correlated with pericyte coverage. (**J**) dP/dt min was measured by left ventricular catheterization (n=10 mice in each group), and (**K**) correlated with pericyte coverage. (**L**) Tau was measured by left ventricular catheterization (n=10 mice in each group). Mann Whitney tests